HHS Public Access

Author manuscript

J Immunol. Author manuscript; available in PMC 2020 May 01.

Published in final edited form as:

J Immunol. 2019 May 01; 202(9): 2760–2771. doi:10.4049/jimmunol.1900039.

Epithelial Expression of an Interstitial Lung Disease Associated Mutation in Surfactant Protein-C Modulates Recruitment and Activation of Key Myeloid Cell Populations in Mice

Alessandro Venosa[1], **Jeremy Katzen**[1], **Yaniv Tomer**[1], **Meghan Kopp**[1], **Sarita Jamil**[1], **Scott J. Russo**[1], **Surafel Mulugeta**[1,2], and **Michael F. Beers**[1,2,†,¶]

[1]Pulmonary, Allergy, and Critical Care Division, Department of Medicine, Perelman School of Medicine, University of Pennsylvania, Philadelphia, Pennsylvania

[2]PENN Center For Pulmonary Biology, University of Pennsylvania, Perelman School of Medicine, Philadelphia, Pennsylvania

Abstract

Patients with idiopathic pulmonary fibrosis (IPF) often experience precipitous deteriorations, termed “acute exacerbations” (AE), marked by diffuse alveolitis and altered gas exchange resulting in significant loss of lung function or mortality. The missense isoleucine to threonine substitution at position 73 [I73T] in the alveolar type-2 cell-restricted Surfactant Protein-C [SP-C] gene [*SFTPC*], has been linked to clinical IPF. To better understand the sequence of events that impact AE-IPF, we leveraged a murine model of inducible SP-C^{I73T} (*SP-C$^{I73T/I73T}$Flp$^{+/-}$*) expression. Following administration of tamoxifen to 8–12 week old mice, an upregulation of *Sftpc^{I73T}* initiated a diffuse lung injury marked by increases bronchoalveolar lavage fluid (BALF) protein and histochemical evidence of CD45^{+} and CD11b^{+} cells infiltrates. Flow cytometry of collagenase digested lung cells revealed a transient, early reduction in SiglecF^{hi}CD11b^{low}CD64^{hi}CD11c^{hi} macrophages, countered by sequential accumulation of SiglecF^{lo}CD11b^{+}CD64^{-}CD11c^{-}CCR2^{+}Ly6C^{+} immature macrophages (3 days), Ly6G^{+} neutrophils (7 days) and SiglecF^{hi}CD11b^{hi}CD11c^{lo} eosinophils (2 weeks). By mRNA analysis, BALF cells demonstrated a time dependent phenotypic shift from a pro-inflammatory (3 days) to an anti-inflammatory / profibrotic activation state, along with serial elaboration of monocyte and eosinophil recruitment factors. Intravenous administration of clodronate effectively reduced total BALF cell numbers, CCR2^{+} immature macrophages, and eosinophil influx while improving survival. In contrast, resident macrophage depletion from intratracheal delivery of clodronate liposomes enhanced *Sftpc^{I73T}* induced mortality. These results using *Sftpc^{I73T}* mice provide a detailed ontogeny for AE-IPF driven by alveolar epithelial dysfunction that induces a polycellular inflammation initiated by the early influx of pro-inflammatory CCR2^{+}Ly6C^{hi} immature macrophages.

[¶]**Correspondence should be addressed to: Michael F. Beers, M.D.**, Pulmonary and Critical Care Division, University of Pennsylvania School of Medicine, Edward J Stemmler Hall, Suite 216, 3450 Hamilton Walk, Philadelphia, Pennsylvania 19104-5159, mfbeers@pennmedicine.upenn.edu.

[†]Albert M. Rose Established Investigator of the Pulmonary Fibrosis Foundation

Conflict of Interest: The authors declare that no conflict of interest exists

INTRODUCTION

Idiopathic pulmonary fibrosis (IPF) is a devastating interstitial lung disease (ILD) characterized by disruption of distal lung architecture that ultimately leads to scar formation, abnormal gas exchange, and respiratory failure. The IPF lung is marked by the pathognomonic histology of Usual Interstitial Pneumonitis (UIP) composed of temporally and spatially heterogeneous areas of fibroblast/myofibroblast accumulation coupled with extracellular matrix deposition, disrupted alveolar architecture, and subpleural honeycombing (1–3). In part, due to incomplete understanding of its pathogenesis, the current "gold-standard" therapy is based on "antifibrotic" (i.e. Pirfenidone; Nintedanib) strategies) which at best only slow the deterioration in pulmonary function (4)

While initial preclinical and translational modeling focused on aberrant mesenchymal expansion in IPF pathogenesis, alveolar type-2 (AT2) epithelial cell dysfunction has re-emerged as a key mechanism driving aberrant lung remodeling through refined crosstalk with all parenchymal populations (5). This notion is bolstered by epidemiological studies and case reports that identified both inherited and sporadic monogenetic mutations in key genes related to telomere length and pulmonary surfactant system proteins (3, 6). Over 60 mutations in the surfactant protein C (SP-C) gene (*SFTPC*), an AT2 specific product, have been described in both adult and pediatric ILD patients. Functionally, SP-C is known to intimately interact with surfactant lipids due to its hydrophobic structure resulting in surface tension modulation in the distal lung. The missense substitution (g.1286T>C), resulting in a change of isoleucine to threonine at position 73 in the SFTPC proprotein ("SP-C^{I73T}"), represents the most common human ILD mutation (7). *In vitro* studies of epithelial cell lines expressing mutant SP-C^{I73T} offered mechanistic insights into the cellular changes seen in *SFTPC*^{I73T} patients, which were each marked by organellar disruption, defective proteostasis, and disruption of cell survival pathways (macroautophagy and mitophagy) (8). To link epithelial dysfunction with fibrotic remodeling *in vivo*, we developed a novel preclinical allelic knock-in murine model designed to express mutant *Sftpc*^{I73T} in an inducible manner (9), thus allowing temporal characterization of key pathways and cellular constituents that drive the aberrant injury/repair response.

Acute exacerbations represent severe clinical deteriorations in patients with chronic ILD (AE-ILD or AE-IPF) that are associated with a high mortality and characterized by extensive inflammatory cell infiltrates, hypoxic respiratory failure, and histological evidence of diffuse alveolar damage superimposed upon the existing PF pathology. Loss of pulmonary function and increased fibrogenic burden represent key downstream effects associated with survivors, corroborating the notion that components of innate and/or adaptive immunity can contribute to aberrant lung remodeling. Although longitudinal data from IPF cohorts are challenging to acquire, analysis of bronchoalveolar lavage fluid (BALF) has shown that elevated levels of chemokines involved in myeloid cell recruitment (MIP-3, CCL22, and CCL17) correlate with poor disease outcomes (10–12). These biomarkers have also been observed in several preclinical models of lung fibrosis (13, 14), therefore supporting the notion that peripheral myeloid cells mobilized during inflammation have the potential to persist in the tissue and participate in lung remodeling (15–18). Given that traditional approaches to AE-PF such as corticosteroids have unproven efficacy (19), a deeper understanding of the immune cell

dynamics driving tissue remodeling are needed to improve efficacy and specificity of current anti-inflammatory strategies.

To address the unmet need for temporal characterization of the inflammation contributing to lung remodeling, the current studies aim to define the sequence of early events resulting in polycellular inflammation during AE-PF. Leveraging the *Sftpc*^{I73T} mouse model, we assessed the ontogeny of the recruitment of these immune cell subsets in lung tissue and BALF following induction of mutant SP-C^{I73T} expression. Furthermore, using depletion protocols, we provide evidence for a key role of peripheral Ly6C^{hi} monocytes in the initiation of the injury. Taken together these studies contribute to a refined understanding of epithelial-immune cell crosstalk in acute episodes of sterile inflammation occurring in PF exacerbations.

MATERIALS AND METHODS

Reagents

Tamoxifen (non-pharmaceutical grade) was purchased from Sigma-Aldrich (St Louis, MO). Clodronate Liposomes were purchased from Encapsula Nanoscience (Encapsula Nanoscience LLC, Brentwood, TN). Giemsa cytological stain was purchased from Sigma-Aldrich. Antibodies used for immunohistochemical and flow cytometric analysis were: CD45 (1:250, Santa Cruz); Eisoniphil Peroxidase (1:150, Santa Cruz); Myeloperoxidase (1:150, Novus Biologics); iNOS (1:200, Abcam); CD11b (1:1500, Abcam); FIZZ-1 (1:800, Stem Cell Technologies); CD64 (1:250, Bioss Antibodies); CCR2 (1:400, Abcam); CCR4 (1:400, Abcam); CX_3CR1 (Bioss Antibodies); CD16/32 (eBiosciences), CD11b (eFluo450, eBiosciences); Fixable Viability dye (eFluo780, eBiosciences); SiglecF (PE-CF594, BD Biosciences); CD45 (PerCP5.5, Biolegend); CD11c (BV705, Biolegend); Ly6G (AF700, biolegend); Ly6C (BV510, Biolegend); CD64 (PE/Cy7, Biolegend); CD3 (BUV395, Biolegend); CD43 (PE, Biolegend); CCR2 (AF647, Biolegend). All other reagents were purchased from Thermo Fisher Scientific, Inc. (Waltham, MA), or Sigma-Aldrich.

Murine Model of Tamoxifen Mediated Sftpc^{I73T} Expression

Tamoxifen inducible SP-C^{I73T}Flp mice were generated as previously reported (9). Briefly the HA-SP-C$^{I73T\text{-}Neo}$ hypomorphic founder line was crossed with a mouse line expressing a FLPe recombinase variant (Flp-O) under control of the mutated ER2 receptor knocked into the Rosa26 locus (Jackson Laboratory, Bar Harbor, ME) to generate the inducible-SP-C^{I73T}Flp line. Tamoxifen treatment of adult SP-C$^{I73T/I73T}$Flp$^{+/-}$ mice was initiated at 8–12 weeks of age. Both male and female animals were used for the studies. Control groups mice are represented as pooled data from tamoxifen treated SP-C$^{I73T/I73T}$Flp$^{-/-}$ genotypes or vehicle (oil) treated SP-C$^{I73T/I73T}$Flp$^{+/-}$mice. All mice were housed under pathogen free conditions in an AALAC approved barrier facility at the Perelman School of Medicine, University of Pennsylvania. All experiments were approved by the Institutional Animal Care and Use Committee at the University of Pennsylvania.

Lung Histology and Immunohistochemistry

Whole lungs were fixed by tracheal instillation of 10% neutral buffer formalin at a constant pressure (25 cm H_2O). Following paraffin embedding, 6 uM sections were cut and stained with Hematoxylin & Eosin (H&E) by the Pathology Core Laboratory of Children's Hospital of Philadelphia. Immunostaining of deparaffinized tissue sections was performed as previously described (20). `Briefly, after antigen retrieval using citrate buffer (10.2 mM sodium citrate, pH 6.0, for 20 minutes) and quenching of endogenous peroxidase with 3% hydrogen peroxide in methanol (30 minutes), non-specific binding was blocked with 10% goat or rabbit serum according to primary antibody origin. Appropriate serum/IgG controls each diluted in blocking buffer were applied for overnight incubation at 4°C in a humidified chamber. Following incubation with biotinylated secondary antisera (Vectastain Elite ABC kit, Vector Labs, Burlingame, CA) for 30 minutes (room temperature), staining was visualized using a Peroxidase Substrate Kit DAB (Vector Labs) and counterstained with Harris Modified Hematoxylin (Thermo Fisher Scientific, Inc.).

Measurement of Pulmonary Function

Invasive measurement of inspiratory capacity and static lung compliance was performed as part of a terminal harvest. Mice were anesthetized with intraperitoneal pentobarbital, tracheas cannulated with a 18-gauge metal stub adapter, and connected to a small-rodent Flexi Vent ventilator (SCIREQ, Inc. Toronto, Ontario CA). Following establishment of standardized basal ventilatory support at a respiratory rate of 150 breaths per min and a tidal volume of 10 mL/kg of body weight, static lung compliance was measured (using PVs-P [27 cmH2O] maneuver) utilizing the manufacturer's software.

Bronchoalveolar Lavage Fluid (BALF) Analysis

BALF was collected from mice using five sequential lavages of 1 ml sterile saline ad processed for analysis as previously described (9). Briefly, cell pellets obtained by centrifuging BALF samples at 400 × *g* for 6 minutes were re-suspended in 1 ml of PBS, and total cell counts determined using a NucleoCounter (New Brunswick Scientific, Edison, NJ). Differential cell counts were determined manually from BALF cytospins stained with modified Giemsa for 20 minutes to identify macrophages, lymphocytes, eosinophils and neutrophils. Total protein content of cell free BALF was determined by the Bradford method with bovine IgG as a standard as described (9).

Cytokine Analysis

First-return aliquots of cell-free BALF were analyzed for CX_3CL1 levels using a Luminex platform (Millipore Sigma, Burlington, MA) by the Human Immunology Core at Perelman School of Medicine.

Flow Cytometry and Cell Sorting For Identification of Immune Populations

Following BALF collection, lungs were cleared of blood by cardiac perfusion with saline solution, removed from the chest cavity, minced, and transferred into a 50 ml conical tube and incubated (37°C, 30') in DMEM + 5% FBS + 2 mg/ml Collagenase D (Cat #11088866001, Roche, Indianapolis, IN). Digested lungs were passed through 70-μm nylon

mesh to obtain a single-cell suspension, counted and mixed with ACK Lysis Buffer (Thermo Fisher Scientific) to remove any remaining red blood cells. BALF and tissue cell pellet ($5X10^5$ cells) were resuspended in 100μl staining buffer (PBS+0.1% sodium azide) and incubated with anti-mouse CD16/32 antibody (Fc block, eBiosciences, San Diego, CA) for 10 min at 4°C to block nonspecific binding. This was followed by 30-min incubation with fluorescently-tagged antibodies or appropriate isotype controls (0.25–1.5 μg/10^6 cells) for 30 minutes (4ºC). Cells were then spun and resuspended in staining buffer for viability staining (30 minutes at 4ºC). Cells were fixed in 2% paraformaldehyde and analyzed with an LSR Fortessa (BD Biosciences, San Jose, CA) or FACS ARIA (BD Biosciences) for cell sorting experiments. Immune cells were identified by forward and side scatter followed by doublet discrimination of $CD45^+$ viable cells. Specific subsets were identified using a gating strategy modified from Misharin, et al (21) as we have published (9), using FlowJo software (FlowJo, LLC, Ashland, Oregon).

Quantitative Real-Time Polymerase Chain Reaction

RNA extracted from BALF cell pellets was purified using RLT buffer and used as template for cDNA preparation using the RetroScript Kit (Qiagen, Valencia, CA) following the manufacturer's protocol. Quantitative single-plex polymerase chain reactions (qPCR) were performed using Taq polymerase and TaqMan qPCR kits (Applied Biosystems/ Thermo Fisher Scientific) on a QuantStudio 7 Flex Real-Time PCR System. The commercial primer sets (all from Applied Biosystems / Thermo Fisher Scientific) were: *Ccl2* (MCP-1) (catalog #Mm00441242_m1), *Ccl17* (TARC) (catalog #Mm01244826_g1), *Cxcl1* (GroA/KC) (catalog #Mm04207460_m1), *Il6* (catalog #Mm00446190_m1), *Il5* (catalog #Mm00439646_m1), *Ccl11* (eotaxin) (catalog #Mm0041238_m1), and *18s* (catalog #Mm03928990_g1). Results are expressed as relative quantities of RNA (versus untreated or wild type controls) after normalization of all values to the corresponding *18s* RNA content.

Macrophage Depletion

Clodronate, encapsulated in liposomes, was used to deplete monocytes/macrophages in blood and lung (22). Control liposomes contained phosphate-buffered saline (PBS) only. For intratracheal treatment each animal received 50 μL (5 mg of clodronate per mL of total suspension volume) of clodronate or control liposomes. For intravenous administration, mice were restrained so that the tail vein was accessible and an insulin syringe was used to administer liposomes (150 mg/kg), 2 h after i.p. tamoxifen injections.

Statistics

All data are presented with dot-plots and group mean ± SEM unless otherwise indicated. Statistical analyses were performed with GraphPad Instat (GraphPad Software, San Diego, CA). Student's t-test were used for paired data; for analyses involving multiple groups, one-way or two way analysis of variance (ANOVA) was performed with post hoc testing as indicated, and survival analyses performed using Log Rank (Mantel-Cox) test. In all cases statistical significance was considered at $p \leq 0.05$.

RESULTS

SP-C^{I73T} expression results in an influx of inflammatory cells into the lung.

Induction of mutant SP-C^{I73T} expression by intraperitoneal tamoxifen administration resulted in significant changes in lung histology, barrier function, and physiology. Whereas minimal histological changes were observed at 3 days post-induction, marked increases in alveolar septal thickening accompanied by epithelial hyperplasia were notable beginning at 7 days (Fig. 1A). In addition, time-dependent increases in alveolar septal disruption, tissue edema, and hemorrhage occurred in association with increased perivascular cellularity. Consistent with prior observations (9), we also found increased BALF total protein at 7 days post induction, along with reduced total inspiratory capacity and increased tissue stiffness, as measured by quasistatic lung compliance (Table 1).

These alterations were accompanied by increases in BALF cell counts, highlighting a mounting inflammatory response that peaked at 2 weeks post tamoxifen (Table 1). This finding was mirrored by immunohistochemistry showing accumulation of CD45$^+$ cells in the lung tissue (Fig. 1B, left panels) and perivascular clusters of CD11b$^+$ immune cells, suggesting their peripheral origin (Fig. 1B, center panels). Using the Fc receptor CD64 as a marker of macrophage maturity, early time dependent decreases in fully differentiated macrophages were observed for up to 2 weeks (Fig. 1B, right panels).

Induction of SP-C^{I73T} expression results in monocyte recruitment and a shift in macrophage polarization towards an anti-inflammatory phenotype.

Examination of BALF cytospins obtained from SP-C^{I73T} mice post tamoxifen treatment revealed dynamic changes in a mixed population of effector cells occurring over the course of 2 weeks (Supp. Fig. 1). To further characterize these cells, BALF and digested lung tissue were each analyzed by flow cytometry utilizing a previously described antibody panel and sorting strategy (9, 21) to identify resident SigF$^+$CD11b$^-$ alveolar macrophages, Ly6G$^+$ neutrophils, SigF$^+$CD11c$^-$ eosinophils, CD3$^+$ lymphocytes, and Ly6C^{hi} immature macrophages (Fig. 2). Correct population gating was validated using Giemsa staining of FACS derived cytospins (Fig. 2, **insets**).

Using this strategy, we first observed a significant diminution of SigF$^+$CD11c$^+$ CD64$^+$CD11b$^-$ alveolar macrophages in BALF and lung tissue digests within 3 days of SP-C^{I73T} induction (Fig. 3A and Supp. Fig. 2B). Whereas the number of these cells returned to control levels by 7 days in the BALF, their relative abundance continued to remain low for up to 2 weeks in the lung tissue (Supp. Fig. 2B). Conversely, BALF and tissue Ly6C$^+$ immature macrophages were increased during this same early inflammatory phase (Fig. 3B and Supp. Fig. 2B). Previously we had shown that SP-C^{I73T} expression increased BALF levels of cytokines involved in the recruitment of monocytes and activated macrophages (CCL2; CCL17) which was mirrored by similar changes in cytokine mRNA expression in AT2 cells (9). qPCR analysis of BALF immune cells indicate that these populations also contribute to *Ccl2/Mcp1* production (Fig. 3C) whereas *Ccl17* mRNA expression remained unchanged 3 days and 2 weeks following mutant *SP-C^{I73T}* induction (Fig. 3D). Immunohistochemical analysis of lung sections also showed increased expression of the

CCL17 receptor, CCR4, on macrophages at 3 days and returned to control levels at 2 weeks (Fig. 3E). By comparison, progressive increases in numbers of $CCR2^+$ mononuclear cells in the lung were found beginning 3 days post induction, while CCR2 expression was absent on neutrophils and eosinophils (Fig. 3F). Similarly, numbers of monocytes/macrophages expressing the chemokine receptor CX_3CR1 were incrementally increased in the lung during the evolution of injury (Fig. 3G), mirrored by commensurate increases in BALF levels of its ligand CX_3CL1 (Fig. 3H).

Macrophages are known to participate in both acute lung injury and resolution/fibrosis (23). Therefore, we sought to temporally define phenotypic changes that occurred after $SP\text{-}C^{I73T}$ induced injury. To this end, we measured mRNA expression of markers canonically associated with pro-inflammatory (M1; inducible nitric oxide synthase [*Nos2*]*; Il6*) and anti-inflammatory/profibrotic (M2; *Arg1*, *Fizz1*) polarization. Due to low baseline expression of inflammatory genes, we expressed quantitated gene expression based on their delta-cycle threshold (dCt) relative to the reference gene 18s (lower dCT ~ higher expression). Although M1 gene expression was increased starting at 3 days after tamoxifen administration, the most dynamic changes observed were on M2 macrophage markers including *Arg1* and *Fizz1* at later time points (2 weeks) (Fig. 4A). Using $2^{-\Delta\Delta Ct}$ method, we also measured *Arg1:Nos2* expression ratio, a surrogate for macrophage activation (24, 25), and found time dependent shift to an anti-inflammatory state (3 days ratio = 10.0; 7 days ratio = 30.4; 2 weeks ratio = 72.7). We further validated these findings at the protein level by staining lung sections and cytospins for iNOS, as well as FIZZ1. Consistent with mRNA analysis, there was upregulation of iNOS in BALF macrophages at 3 days, which persisted up to 2 weeks (Fig. 4B). Conversely, staining for M2 markers increased steadily through the first 2 weeks (Fig. 4C).

$SP\text{-}C^{I73T}$ expression promotes a multiphasic and multicellular alveolitis.

Using the same gating strategy (Figure 2), analysis of BALF and tissue-derived cells both demonstrated a steady accumulation of $Ly6G^+$ neutrophils peaking at 7 days (Fig. 5A and Supp. Fig. 2B) and $SigF^+CD11c^-$ eosinophils, peaking at 2 weeks (Fig. 5D and Supp. Fig. 2B). Consistent with these findings, immunohistochemical staining of tissue sections showed increased numbers of myeloperoxidase (MPO) positive neutrophils at 7 days (Fig. 5B), as well as eosinophil peroxidase (EPX) positive eosinophils 2 weeks post induction (Fig. 5E). Furthermore, consistent with our BALF differential analysis, the number of BALF $CD3^+$ cells also steadily increased, though the relative percentage of these cells remained unchanged in the tissue (Suppl. Fig. 2A).

As previous work from our group identified a central role for epithelial cells in the early recruitment of peripheral subsets of these granulocytes through elaboration of key cytokines (9), we sought to determine whether BALF immune cells could also participate in this process. Interestingly, while BALF cells were not a source of *Cxcl1* (Fig. 5C), we did observe increased and persistent expression of *Ccl11/Eotaxin* and *Il5* up to 2 weeks post-tamoxifen (Fig. 5F).

Peripheral monocyte depletion alters the injury course by improving survival and reducing cell influx in SP-C^{I73T} mice.

As a result of this detailed temporal characterization, we identified peripheral Ly6C^{hi} monocytes as the first peripheral subset infiltrating into the tissue through activation of the MCP-1/CCR2 axis and hypothesized that their participation was crucial in driving lung injury and alveolitis caused by *Sftpc^{I73T}* expression. We next tested whether pharmacological depletion of resident alveolar macrophages or peripheral monocytes with control (CL) and clodronate loaded liposomes (CLOD) would alter the course of early and late inflammatory processes. Consistent with a role of resident macrophages in maintenance of homeostasis, depletion of alveolar macrophages using intratracheal CLOD resulted in a significant increase in mortality within 7 days post *Sftpc^{I73T}* induction (Fig. 6A). At this time point, while histological analysis of lungs from tamoxifen induced mice showed relatively mild cellular infiltration, resident macrophage depletion revealed extensive parenchymal remodeling and appearance of conspicuous pockets of inflammatory cells, resembling bronchoalveolar lymphoid tissue (BALT) (Fig. 6B). Of note, neither control nor clodronate loaded liposomes affected lung architecture. Conversely, intravenous delivery of clodronate liposomes, previously shown to alter peripheral monocyte homeostasis, resulted in enhanced survival post *Sftpc^{I73T}* induction (90% TAM+CLOD vs. 54% TAM, at 2 weeks) (Fig. 6C). This protective effect on mortality was reflected in the histology with animals receiving i.v. CLOD demonstrating reduction in inflammatory cells particularly in the alveolar and perivascular regions and overall attenuation of parenchymal lung damage (Fig. 6D). The blunted inflammatory response was also reflected in diminished numbers of total BALF cells in mice treated at both 7 days and 2 weeks post tamoxifen induction (Fig. 6E).

Intravenous clodronate effectively reduces accumulation of Ly6C^{hi}CCR2^{+} immature macrophages and eosinophils in the lungs of Sftpc^{I73T} expressing mice.

The protective effects of systemic clodronate (i.v. CLOD) administration on the early injury were reflected in alterations in the dynamics of the immune cell composition of BALF and lung tissue. As noted previously, induction of *Sftpc^{I73T}* mutant was associated with early reduction in SigF^{+}CD11b^{-} alveolar macrophages paired with increased Ly6C^{hi} immature macrophages in the BALF (Fig. 3). Systemic clodronate had no effects on alveolar macrophage numbers in BALF (Supp. Fig. 3A) and tissue digests (data not shown). Conversely, i.v. CLOD resulted in reduced immature macrophage numbers in the BALF during the early (3 days) inflammatory phase, but not in total Ly6C^{hi} cells in the tissue (Figs. 7A, 7C). Further analysis on Ly6C^{hi} immature macrophages subpopulations revealed that CLOD had significant effects on BALF and tissue burden of pro-inflammatory Ly6C^{+}CCR2^{+} immature macrophages at 3 days (Figs. 7B, 7D). Histochemical analysis of lung sections further confirmed reduction of CCR2^{+} cells in SP-C^{I73T} induced mice following CLOD treatment (Fig. 7E). Additional qPCR analysis of recovered BALF immune cells showed that CLOD treated *Sftpc^{I73T}* mice exhibited no alteration in the gene expression of factors involved in monocyte recruitment (*Mcp1*), nor macrophage activation (*Fizz1*, *Arg1*, *Nos2,* and *Il6*) (Supp. Fig. 4). CLOD depletion also had no effect on neutrophil infiltration (Sup. Fig. 3B), while there was significant reduction in eosinophils in both BALF and tissue at 2 weeks assessed by flow cytometry analysis of SigF^{+}CD11c^{-} cells (Figs. 8A, 8B), as well as immunohistochemistry for eosinophil peroxidase (EPX) (Fig. 8C).

DISCUSSION

Mutations of the *SFTPC* gene have been linked to various forms of diffuse parenchymal lung disease (DPLD) in humans, namely idiopathic pulmonary fibrosis (IPF) and chILD in adults and pediatric patients, respectively. The clinical course of these DPLDs is often punctuated by acute exacerbations (AE) which are marked by overt spikes in the inflammatory burden to the lung associated with high mortality from superimposed acute lung injury which often results in a significant reduction of pulmonary function among survivors (26). There is an unmet need for new therapies for IPF/ILD due to incomplete understanding of the pathogenesis of both the underlying fibrosis and acute exacerbations, as prior pharmacological interventions (corticosteroids, cytokine modulation, anti-fibrotics) have focused on attenuating downstream responses that at best result in delay, rather than prevention, of pulmonary function decline (27–29).

Part of this challenge to development of effective therapies has been the absence of preclinical experimental models that translate to IPF/chILD patients. Our laboratory has recently developed two murine models of spontaneous pulmonary fibrosis each driven by a distinct functional class of *SFTPC* mutation that localize within either the BRICHOS (C121G mutant) or 'linker' (I73T) domains of the SP-C proprotein (9, 30). Mutant SFTPC BRICHOS isoforms are misfolded and produce extensive AT2 ER stress and apoptosis (30). In contrast, Non-BRICHOS mutants such as $SFTPC^{I73T}$ mistraffic to the AT2 plasma membrane, accumulate in late endosomes, and generate a different toxic gain of function AT2 cell phenotype marked by an acquired block in macroautophagy and hyperproliferation (8–9). Importantly, although expression of these two mutants result in divergent molecular, biochemical, and cellular phenotypes, each is characterized by an overlapping lung phenotype which includes inflammation and extensive tissue remodeling that established a central role for AT2 cells in the initiation of the inflammatory response through release of a diverse array of factors involved in recruitment and activation of immune cell subsets. Herein, the present work extends these prior observations as we now utilize the $SP\text{-}C^{I73T}$ Non-BRICHOS model to temporally define and characterize the role of resident (alveolar macrophages) and peripheral (monocytes, neutrophils, and eosinophils) immune cell subsets accumulating in the lung prior to and during the alveolitis, parenchymal injury, lung injury and early remodeling following the induction of mutant $Sftpc^{I73T}$ expression. Furthermore, utilizing clodronate depletion we establish a detrimental role for pro-inflammatory $Ly6C^{+}$ monocytes in injury progression.

Understanding the AT2-immune cell crosstalk coordinating both recruitment of $CD45^{+}$ effector cells and systemic inflammation is pivotal to expanding and validating new therapeutic paradigms for IPF and chILD. A large part of our understanding of the mechanisms of acute and chronic inflammatory lung disease is the product of experimental models that rely on exogenous exposures (ozone, LPS, or bleomycin) which can non-specifically affect a myriad of parenchymal subsets. Conversely, the $SP\text{-}C^{I73T}$ model represents a new and clinically relevant approach to characterize endogenous sterile inflammation and fibrogenesis initiated by epithelial cell stress (9, 31). Leveraging this approach, the induction of mutant $Sftpc^{I73T}$ expression was associated with an initial tissue inflammatory response (Fig. 1) in association with a transient decrease in $SigF^{+}CD11b^{-}$

resident alveolar macrophages (Fig. 2). Alveolar macrophages represent the first line of defense against pathogen exposure and may be important for maintaining homeostasis of the alveolar niche, a response achieved in coordination with the lung epithelium and mesenchyme (32, 33). Due to their extensive phenotypic plasticity through adaption to the surrounding chemical milieu (34, 35), macrophages have been classified into two major activation states: classically activated (M1) macrophages, essential in the early response to pro-inflammatory signals (TNF-α, IFN-γ); and alternatively activated (M2) macrophages, important in termination of inflammation as well as in tissue remodeling following Th2 stimulation (IL-10, TGF-β, IL-4 and IL-13) (23). Consistent with this notion we found sequential M1 (3 d; *Nos2, Il6*) and M2 (2 wk; *Arg1, Fizz1*) activation following induction of mutant *Sftpc*^{I73T} expression (Fig. 4). It remains to be determined whether the change in activation status observed over time is the result of phenotypic shift of resident macrophages, influx of activated peripheral subsets or rather a combination of the two which will be elucidated in future studies.

Under homeostatic conditions, the alveolar macrophage pool self-maintains through proliferation (36), while a combination of recruitment and maturation of peripheral monocytes is indispensable to overcome loss of resident subsets following injury (37, 38). Bone marrow chimeras and monocyte reporter mice have been necessary to pinpoint and study the phenotypic changes taking place during the shift from monocyte, to immature macrophages, and ultimately mature alveolar macrophage (15, 39). In accord with this notion, the initial reduction in BALF and tissue CD11c^{+}CD64^{+}SigF^{+}CD11b^{-} alveolar macrophages upon SP-C^{I73T} mutant protein induction was countered by accumulation of CD11b^{+}Ly6C^{hi} immature macrophages. This immature myeloid subset was previously shown to be recruited through a CCL2/MCP-1 axis (40) and is congruent with our previous findings of increased MCP-1 levels in the BALF within 3 days post-induction of the SP-C^{I73T} mutant (9). Although the BALF levels of CCL2/MCP-1 returned to control values by 7 days, we found sustained *Ccl2* transcript levels in epithelial and immune cells, accompanied by the steady accumulation of CD11b^{+}Ly6C^{hi}CCR2^{+} immature macrophages in the lung for up to 2 weeks (Fig. 3B and 3F). While this could likely generate a more localized gradient for CCL2/MCP-1 not detectable in whole BALF, we cannot exclude the existence of parallel monocyte recruitment signals. Indeed, our results support this notion by showing increased levels of CCL17 protein and CCR4 expression, thus complementing previous cytokine analysis proposing CCL17/CCR4 axis participation in the development of a non-canonical M2/Th2 inflammatory phenotype (9) in clinical IPF (12, 41). Our data also show that while both epithelial and immune cells can contribute to persistent CCL2/MCP-1 production (9), AT2 cells were the sole source of *Ccl17* expression, thus confirming a central role for the epithelium in the immune response in this model and likely in clinical IPF (10, 12, 13).

As monocytes were the first peripheral population recruited in the lung following SP-C^{I73T} induction (Fig. 3), we asked whether disruption of this process could alter injury progression. Intratracheal (i.t.) and intravenous (i.v.) clodronate liposomes represent widely used experimental methodologies to reduce monocyte/macrophage numbers in the compartment of interest (42). Although its mechanism of action is not targeted to specific macrophage subsets, neither route of administration has been shown to affect interstitial cells

(43, 44). Perhaps one of the most interesting findings to emerge from this work is represented by the dichotomous effects of clodronate depending upon route of administration. Notable was observation that resident alveolar macrophage depletion, resulted in significantly decreased survival (Fig. 6A), that was accompanied by histological evidence of severe inflammation within 6 days of SP-C^{I73T} induction (Fig. 6B). At higher power, we noted the presence of clusters of neutrophils and lymphocytes. The morphology of these lesions is consistent with a possible acquisition of induced Bronchus-associated Lymphoid Tissue (iBALT), however its definitive identification will require microdissection and flow cytometric characterization of these regions to properly define such structures as published by Harmsen's group (45). Regardless, the current data intriguingly suggest a pivotal role for resident alveolar macrophages in lung immune homeostasis and in containing the inflammatory burst that develops in response to mutant SP-C^{I73T} induction in AT2 cells (Fig 6B).

Conversely, we found that when systemically administered, clodronate effectively blunted the accumulation of CCR2^{+}Ly6C^{+} immature macrophages during acute injury, while also significantly improving overall survival and modulating inflammatory endpoints such as total BALF cell numbers, CCR2^{+} cell influx, and expansion of eosinophils (Figs. 6 and 7). These findings suggest that recruitment of this blood borne subset plays a deleterious role early in SP-C^{I73T} lung injury, a notion consistent with other experimental models of acute and chronic injury in the lung and elsewhere (15, 46, 47). In addition, our data are consistent with findings indicating a pro-inflammatory and pro-injurious function of peripheral monocytes due, at least in part, to their distinct ontogeny from that of resident macrophages (48). This notion is further supported by experimental models of bleomycin-induced injury showing significant contributions of monocyte-derived alveolar macrophages to the aberrant injury and remodeling (15).

In this model, we observed a consistent and well defined dynamic accumulation of eosinophils in tissue and BALF after tamoxifen induced *Sftpc^{I73T}* induction (Fig. 5D; Supp. Fig. 2B). An exhaustive literature describes the role of eosinophils in parasitic infection, allergic disease, and asthma (49, 50). Complementary, clinical evidence has clearly established eosinophil presence in several subtypes of DPLD including IPF (18, 51, 52) and in acute exacerbations (53), however their exact functions are currently unknown. Eosinophils have been shown to promote parenchymal destruction via release of highly toxic granules containing hypobromite, superoxide, and peroxide; yet, they are also source of hematopoietic and growth factors involved in tissue remodeling/fibrosis (e.g. TGF-β) (54, 55). Using this model we previously showed that AT2 epithelial cells represent a source of cytokines associated with eosinophil recruitment (CCL11) and maintenance (IL-5) upon induction of SP-C^{I73T} (9). In the current studies we show by qPCR that BALF immune cells also participate in eosinophil mobilization albeit at a later time point (2 weeks), suggesting they may act to amplify ongoing inflammatory cell recruitment. Notably, as Ly6C^{+} monocytes have been shown to recruit eosinophils in a CCL11-dependent manner (56), our observations that peripheral monocyte depletion results in reduced eosinophil numbers in the lung after SP-C^{I73T} mutant induction further support the notion that these cells could be important in injury progression.

Through analysis of both tissue and BALF, we demonstrated that these compartments are comparable when characterizing mobile effector cell subsets and for which BALF analysis in patients with a variety of ILDs has often been used to assess disease activity. However, due to the complexity of acute exacerbations, analysis of tissue digests offers additional information of interstitial populations that may contribute to injury initiation and progression. While our data has focused on the role of myeloid immune cell populations, it is likely that effector cells of lymphoid origin such as regulatory T cells, or the recently characterized lineage negative innate lymphoid cells (ILCs), could also play a role. In support to this notion, T_{regs} have been previously shown to participate to both acute exacerbations of lung disease and aberrant lung remodeling (57, 58), while ILC2s, despite their elusive nature, have been heavily linked with pulmonary disease states enriched in non-canonical Th2 factors (i.e., IL-5, IL-6 and IL-13) (59, 60). Based on our findings of conspicuous levels of these cytokines after SP-C^{I73T} mutant induction, it is intriguing to propose that this regulatory subset could play a role in the dynamic inflammatory events associated with this preclinical model.

In summary, using a novel model of endogenous, sterile lung injury, the present study demonstrates that expression of a mutant *Sftpc* protein in the pulmonary epithelium of mice recapitulates many features of acute exacerbations of DPLD in human patients. In addition to characterizing the ontogeny of the immune cell response to AT2 cell stress, these results offer important insight into the role of peripheral pro-inflammatory monocytes in the initiation and amplification/progression of inflammatory events in ILD pathogenesis. The complexity of the effector cell cascades observed during SP-C^{I73T} induced acute exacerbations supports the notion that a multi-target therapeutic approach will be required to make significant inroads into the treatment of IPF and chILD.

Supplementary Material

Refer to Web version on PubMed Central for supplementary material.

ACKNOWLEDGEMENTS

The authors thank Drs. Debra Laskin, and Andrew Gow for valuable input. MF Beers is the Albert M. Rose Established Investigator of the Pulmonary Fibrosis Foundation.

Grant Support: VA Merit Review 1I01BX001176 (MFB), NIH RO1 HL119436 (MFB), NIH P30 ES013508 (MFB) and HL129150 (SM); JK was supported by NIH 2T32 HL007586

Non-Standard Abbreviations:

AT2	alveolar type-2 cell
BRICHOS	Bri family of proteins
Sftpc^{I73T}	surfactant protein-C I73T mutant
HA	hemaglutinin antigen protein
ILD	interstitial lung disease

IPF	idiopathic pulmonary fibrosis
BALF	bronchoalveolar lavage fluid
FACS	fluorescence-activated cell sorting
CLOD	clodronate liposomes

REFERENCES

1. Cameron HS, Somaschini M, Carrera P, Hamvas A, Whitsett JA, Wert SE, Deutsch G, and Nogee LM. 2005 A common mutation in the surfactant protein C gene associated with lung disease. J Pediatr 146: 370–375. [PubMed: 15756222]
2. Abou Taam R, Jaubert F, Emond S, Le Bourgeois M, Epaud R, Karila C, Feldmann D, Scheinmann P, and de Blic J. 2009 Familial interstitial disease with I73T mutation: A mid- and long-term study. Pediatr Pulmonol 44: 167–175. [PubMed: 19148933]
3. Crossno PF, Polosukhin VV, Blackwell TS, Johnson JE, Markin C, Moore PE, Worrell JA, Stahlman MT, Phillips JA 3rd, Loyd JE, Cogan JD, and Lawson WE. 2010 Identification of early interstitial lung disease in an individual with genetic variations in ABCA3 and SFTPC. Chest 137: 969–973. [PubMed: 20371530]
4. Noble PW, Albera C, Bradford WZ, Costabel U, du Bois RM, Fagan EA, Fishman RS, Glaspole I, Glassberg MK, Lancaster L, Lederer DJ, Leff JA, Nathan SD, Pereira CA, Swigris JJ, Valeyre D, and King TE. 2016 Pirfenidone for idiopathic pulmonary fibrosis: analysis of pooled data from three multinational phase 3 trials. Eur Respir J 47: 243–253. [PubMed: 26647432]
5. Selman M, and Pardo A. 2014 Revealing the pathogenic and aging-related mechanisms of the enigmatic idiopathic pulmonary fibrosis. an integral model. Am J Respir Crit Care Med 189: 1161–1172. [PubMed: 24641682]
6. Povedano JM, Martinez P, Flores JM, Mulero F, and Blasco MA. 2015 Mice with Pulmonary Fibrosis Driven by Telomere Dysfunction. Cell Rep 12: 286–299. [PubMed: 26146081]
7. Brasch F, Griese M, Tredano M, Johnen G, Ochs M, Rieger C, Mulugeta S, Muller KM, Bahuau M, and Beers MF. 2004 Interstitial lung disease in a baby with a de novo mutation in the SFTPC gene. Eur Respir J 24: 30–39. [PubMed: 15293602]
8. Hawkins A, Guttentag SH, Deterding R, Funkhouser WK, Goralski JL, Chatterjee S, Mulugeta S, and Beers MF. 2015 A non-BRICHOS SFTPC mutant (SP-C(I73T)) linked to interstitial lung disease promotes a late block in macroautophagy disrupting cellular proteostasis and mitophagy. Am J Physiol Lung Cell Mol Physiol 308: L33–L47. [PubMed: 25344067]
9. Nureki SI, Tomer Y, Venosa A, Katzen J, Russo SJ, Jamil S, Barrett M, Nguyen V, Kopp M, Mulugeta S, and Beers MF. 2018 Expression of mutant Sftpc in murine alveolar epithelia drives spontaneous lung fibrosis. J Clin Invest 128: 4008–4024 [PubMed: 29920187]
10. Shinoda H, Tasaka S, Fujishima S, Yamasawa W, Miyamoto K, Nakano Y, Kamata H, Hasegawa N, and Ishizaka A. 2009 Elevated CC chemokine level in bronchoalveolar lavage fluid is predictive of a poor outcome of idiopathic pulmonary fibrosis. Respiration 78: 285–292. [PubMed: 19270434]
11. Capelli A, Di Stefano A, Gnemmi I, and Donner CF. 2005 CCR5 expression and CC chemokine levels in idiopathic pulmonary fibrosis. Eur Respir J 25: 701–707. [PubMed: 15802346]
12. Yogo Y, Fujishima S, Inoue T, Saito F, Shiomi T, Yamaguchi K, and Ishizaka A. 2009 Macrophage derived chemokine (CCL22), thymus and activation-regulated chemokine (CCL17), and CCR4 in idiopathic pulmonary fibrosis. Respir Res 10: 80. [PubMed: 19715610]
13. Belperio JA, Dy M, Murray L, Burdick MD, Xue YY, Strieter RM, and Keane MP. 2004 The Role of the Th2 CC Chemokine Ligand CCL17 in Pulmonary Fibrosis. J Immunol 173: 4692. [PubMed: 15383605]
14. Inoue T, Fujishima S, Ikeda E, Yoshie O, Tsukamoto N, Aiso S, Aikawa N, Kubo A, Matsushima K, and Yamaguchi K. 2004 CCL22 and CCL17 in rat radiation pneumonitis and in human idiopathic pulmonary fibrosis. Eur Respir J 24: 49. [PubMed: 15293604]

15. Misharin AV, Morales-Nebreda L, Reyfman PA, Cuda CM, Walter JM, McQuattie-Pimentel AC, Chen CI, Anekalla KR, Joshi N, Williams KJN, Abdala-Valencia H, Yacoub TJ, Chi M, Chiu S, Gonzalez-Gonzalez FJ, Gates K, Lam AP, Nicholson TT, Homan PJ, Soberanes S, Dominguez S, Morgan VK, Saber R, Shaffer A, Hinchcliff M, Marshall SA, Bharat A, Berdnikovs S, Bhorade SM, Bartom ET, Morimoto RI, Balch WE, Sznajder JI, Chandel NS, Mutlu GM, Jain M, Gottardi CJ, Singer BD, Ridge KM, Bagheri N, Shilatifard A, Budinger GRS, and Perlman H. 2017 Monocyte-derived alveolar macrophages drive lung fibrosis and persist in the lung over the life span. J Exp Med 214: 2387–2404. [PubMed: 28694385]

16. Obayashi Y, Yamadori I, Fujita J, Yoshinouchi T, Ueda N, and Takahara J. 1997 The role of neutrophils in the pathogenesis of idiopathic pulmonary fibrosis. Chest 112: 1338–1343. [PubMed: 9367478]

17. Gregory AD, Kliment CR, Metz HE, Kim KH, Kargl J, Agostini BA, Crum LT, Oczypok EA, Oury TA, and Houghton AM. 2015 Neutrophil elastase promotes myofibroblast differentiation in lung fibrosis. J Leukoc Biol 98: 143–152. [PubMed: 25743626]

18. Brix N, Rasmussen F, Poletti V, and Bendstrup E. 2016 Eosinophil alveolitis in two patients with idiopathic pulmonary fibrosis. Respiratory Medicine Case Reports 19: 61–64. [PubMed: 27625983]

19. Raghu G, Anstrom KJ, King TE Jr., Lasky JA, and Martinez FJ. 2012 Prednisone, azathioprine, and N-acetylcysteine for pulmonary fibrosis. N Engl J Med 366: 1968–1977. [PubMed: 22607134]

20. Venosa A, Malaviya R, Choi H, Gow AJ, Laskin JD, and Laskin DL. 2015 Characterization of Distinct Macrophage Subpopulations During Nitrogen Mustard-Induced Injury and Fibrosis. Am J Respir Cell Mol Biol

21. Misharin AV, Morales-Nebreda L, Mutlu GM, Budinger GR, and Perlman H. 2013 Flow cytometric analysis of macrophages and dendritic cell subsets in the mouse lung. Am J Respir Cell Mol Biol 49: 503–510. [PubMed: 23672262]

22. Rooijen NV, and Sanders A. 1994 Liposome mediated depletion of macrophages: mechanism of action, preparation of liposomes and applications. J Immunol Methods 174: 83–93. [PubMed: 8083541]

23. Mantovani A, and Sica A. 2010 Macrophages, innate immunity and cancer: balance, tolerance, and diversity. Curr Opin Immunol 22: 231–237. [PubMed: 20144856]

24. Munder M, Eichmann K, Moran JM, Centeno F, Soler G, and Modolell M. 1999 Th1/Th2-regulated expression of arginase isoforms in murine macrophages and dendritic cells. J Immunol 163: 3771–3777. [PubMed: 10490974]

25. Shi JD, Golden T, Guo CJ, Tu SP, Scott P, Lee MJ, Yang CS, and Gow AJ. 2013 Tocopherol supplementation reduces NO production and pulmonary inflammatory response to bleomycin. Nitric Oxide 34: 27–36. [PubMed: 23669183]

26. Hambly N, Cox G, and Kolb M. 2017 Acute exacerbations of idiopathic pulmonary fibrosis: tough to define; tougher to manage. Eur Respir J 49.

27. Behr J, and Richeldi L. 2013 Recommendations on treatment for IPF. Respir Res 14: S6–S6. [PubMed: 23734936]

28. Richeldi L, Davies H, Spagnolo P, and Luppi F. 2003 Corticosteroids for idiopathic pulmonary fibrosis. Cochrane Database Syst Rev

29. Papiris SA, Manali ED, Kolilekas L, Triantafillidou C, Tsangaris I, and Kagouridis K. 2012 Steroids in idiopathic pulmonary fibrosis acute exacerbation: defenders or killers? Am J Respir Crit Care Med 185: 587–588. [PubMed: 22383571]

30. Katzen J, Wagner BD, Venosa A, Kopp M, Tomer Y, Russo SJ, Headen AC, Basil MC, Stark JM, Mulugeta S, Deterding RR, and Beers MF. 2019 A SFTPC BRICHOS mutant links epithelial ER stress and spontaneous lung fibrosis. JCI Insight doi: 10.1172/jci.insight.126125.

31. Blackwell TS 2018 Lung injury and fibrosis induced by a mutant form of surfactant protein C. J Clinl Invest 128: 3745–3746.

32. Herold S, Mayer K, and Lohmeyer J. 2011 Acute Lung Injury: How Macrophages Orchestrate Resolution of Inflammation and Tissue Repair. Front Immunol 2: 65. [PubMed: 22566854]

33. Westphalen K, Gusarova GA, Islam MN, Subramanian M, Cohen TS, Prince AS, and Bhattacharya J. 2014 Sessile alveolar macrophages communicate with alveolar epithelium to modulate immunity. Nature 506: 503–506. [PubMed: 24463523]
34. Liu H, Wu X, Gang N, Wang S, Deng W, Zan L, and Yu S. 2015 Macrophage functional phenotype can be consecutively and reversibly shifted to adapt to microenvironmental changes. Int J Clin Exp Med 8: 3044–3053. [PubMed: 25932281]
35. Stout RD, and Suttles J. 2004 Functional plasticity of macrophages: reversible adaptation to changing microenvironments. J Leukoc Biol 76: 509–513. [PubMed: 15218057]
36. Hashimoto D, Chow A, Noizat C, Teo P, Beasley MB, Leboeuf M, Becker CD, See P, Price J, Lucas D, Greter M, Mortha A, Boyer SW, Forsberg EC, Tanaka M, van Rooijen N, Garcia-Sastre A, Stanley ER, Ginhoux F, Frenette PS, and Merad M. 2013 Tissue-resident macrophages self-maintain locally throughout adult life with minimal contribution from circulating monocytes. Immunity 38: 792–804. [PubMed: 23601688]
37. Epelman S, Lavine KJ, Beaudin AE, Sojka DK, Carrero JA, Calderon B, Brija T, Gautier EL, Ivanov S, Satpathy AT, Schilling JD, Schwendener R, Sergin I, Razani B, Forsberg EC, Yokoyama WM, Unanue ER, Colonna M, Randolph GJ, and Mann DL. 2014 Embryonic and adult-derived resident cardiac macrophages are maintained through distinct mechanisms at steady state and during inflammation. Immunity 40: 91–104. [PubMed: 24439267]
38. Maus UA, Janzen S, Wall G, Srivastava M, Blackwell TS, Christman JW, Seeger W, Welte T, and Lohmeyer J. 2006 Resident alveolar macrophages are replaced by recruited monocytes in response to endotoxin-induced lung inflammation. Am J Respir Cell Mol Biol 35: 227–235. [PubMed: 16543608]
39. Aran D, Looney AP, Liu L, Wu E, Fong V, Hsu A, Chak S, Naikawadi RP, Wolters PJ, Abate AR, Butte AJ, and Bhattacharya M. 2019 Reference-based analysis of lung single-cell sequencing reveals a transitional profibrotic macrophage. Nat Immunol 20: 163–172. [PubMed: 30643263]
40. Gelman AE, Okazaki M, Sugimoto S, Li W, Kornfeld CG, Lai J, Richardson SB, Kreisel FH, Huang HJ, Tietjens JR, Zinselmeyer BH, Patterson GA, Miller MJ, Krupnick AS, and Kreisel D. 2010 CCR2 regulates monocyte recruitment as well as CD4 T1 allorecognition after lung transplantation. Am J Transplant 10: 1189–1199. [PubMed: 20420631]
41. Pignatti P, Brunetti G, Moretto D, Yacoub MR, Fiori M, Balbi B, Balestrino A, Cervio G, Nava S, and Moscato G. 2006 Role of the chemokine receptors CXCR3 and CCR4 in human pulmonary fibrosis. Am J Respir Crit Care Med 173: 310–317. [PubMed: 16239626]
42. van Rooijen N, and Hendrikx E. 2010 Liposomes for specific depletion of macrophages from organs and tissues. Methods Mol Biol 605: 189–203. [PubMed: 20072882]
43. Mathie SA, Dixon KL, Walker SA, Tyrrell V, Mondhe M, O'Donnell VB, Gregory LG, and Lloyd CM. 2015 Alveolar macrophages are sentinels of murine pulmonary homeostasis following inhaled antigen challenge. Allergy 70: 80–89. [PubMed: 25331546]
44. Sabatel C, Radermecker C, Fievez L, Paulissen G, Chakarov S, Fernandes C, Olivier S, Toussaint M, Pirottin D, Xiao X, Quatresooz P, Sirard JC, Cataldo D, Gillet L, Bouabe H, Desmet CJ, Ginhoux F, Marichal T, and Bureau F. 2017 Exposure to Bacterial CpG DNA Protects from Airway Allergic Inflammation by Expanding Regulatory Lung Interstitial Macrophages. Immunity 46: 457–473. [PubMed: 28329706]
45. Richert LE, Harmsen AL, Rynda-Apple A, Wiley JA, Servid AE, Douglas T, and Harmsen AG. 2013 Inducible bronchus-associated lymphoid tissue (iBALT) synergizes with local lymph nodes during antiviral CD4+ T cell responses. Lymphat Res Biol 11: 196–202. [PubMed: 24364842]
46. Sung SA, Jo SK, Cho WY, Won NH, and Kim HK. 2007 Reduction of Renal Fibrosis as a Result of Liposome Encapsulated Clodronate Induced Macrophage Depletion after Unilateral Ureteral Obstruction in Rats. Nephron Exp Nephrol 105: e1–e9. [PubMed: 17106213]
47. Misharin AV, Cuda CM, Saber R, Turner JD, Gierut AK, Haines GK 3rd, Berdnikovs S, Filer A, Clark AR, Buckley CD, Mutlu GM, Budinger GR, and Perlman H. 2014 Nonclassical Ly6C(−) monocytes drive the development of inflammatory arthritis in mice. Cell Rep 9: 591–604. [PubMed: 25373902]
48. Yu X, Buttgereit A, Lelios I, Utz SG, Cansever D, Becher B, and Greter M. 2017 The Cytokine TGF-beta Promotes the Development and Homeostasis of Alveolar Macrophages. Immunity 47: 903–912.e904. [PubMed: 29126797]

49. O'Connell EM, and Nutman TB. 2015 Eosinophilia in Infectious Diseases. Immunol Allergy Clin North Am 35: 493–522. [PubMed: 26209897]
50. Durham SR, and Kay AB. 1985 Eosinophils, bronchial hyperreactivity and late-phase asthmatic reactions. Clin Allergy 15: 411–418. [PubMed: 4053332]
51. Birring SS, Parker D, McKenna S, Hargadon B, Brightling CE, Pavord ID, and Bradding P. 2005 Sputum eosinophilia in idiopathic pulmonary fibrosis. Inflamm Res 54: 51–56. [PubMed: 15750711]
52. Peterson MW, Monick M, and Hunninghake GW. 1987 Prognostic role of eosinophils in pulmonary fibrosis. Chest 92: 51–56. [PubMed: 3595249]
53. Kakugawa T, Sakamoto N, Sato S, Yura H, Harada T, Nakashima S, Hara A, Oda K, Ishimoto H, Yatera K, Ishimatsu Y, Obase Y, Kohno S, and Mukae H. 2016 Risk factors for an acute exacerbation of idiopathic pulmonary fibrosis. Respir Res 17: 79. [PubMed: 27401332]
54. Ohkawara Y, Tamura G, Iwasaki T, Tanaka A, Kikuchi T, and Shirato K. 2000 Activation and transforming growth factor-beta production in eosinophils by hyaluronan. Am J Respir Cell Mol Biol 23: 444–451. [PubMed: 11017908]
55. Tanaka H, Komai M, Nagao K, Ishizaki M, Kajiwara D, Takatsu K, Delespesse G, and Nagai H. 2004 Role of interleukin-5 and eosinophils in allergen-induced airway remodeling in mice. Am J Respir Cell Mol Biol 31: 62–68. [PubMed: 14975941]
56. Waddell A, Ahrens R, Steinbrecher K, Donovan B, Rothenberg ME, Munitz A, and Hogan SP. 2011 Colonic eosinophilic inflammation in experimental colitis is mediated by Ly6C(high) CCR2(+) inflammatory monocyte/macrophage-derived CCL11. J Immunol 186: 5993–6003. [PubMed: 21498668]
57. Birjandi SZ, Palchevskiy V, Xue YY, Nunez S, Kern R, Weigt SS, Lynch JP 3rd, Chatila TA, and Belperio JA. 2016 CD4(+)CD25(hi)Foxp3(+) Cells Exacerbate Bleomycin-Induced Pulmonary Fibrosis. Am J Pathol 186: 2008–2020. [PubMed: 27317904]
58. Hams E, Armstrong ME, Barlow JL, Saunders SP, Schwartz C, Cooke G, Fahy RJ, Crotty TB, Hirani N, Flynn RJ, Voehringer D, McKenzie ANJ, Donnelly SC, and Fallon PG. 2014 IL-25 and type 2 innate lymphoid cells induce pulmonary fibrosis. Proc Natl Acad Sci U S A 111: 367–372. [PubMed: 24344271]
59. Moro K, Yamada T, Tanabe M, Takeuchi T, Ikawa T, Kawamoto H, Furusawa J, Ohtani M, Fujii H, and Koyasu S. 2010 Innate production of T(H)2 cytokines by adipose tissue-associated c-Kit(+)Sca-1(+) lymphoid cells. Nature 463: 540–544. [PubMed: 20023630]
60. Barlow JL, Peel S, Fox J, Panova V, Hardman CS, Camelo A, Bucks C, Wu X, Kane CM, Neill DR, Flynn RJ, Sayers I, Hall IP, and McKenzie AN. 2013 IL-33 is more potent than IL-25 in provoking IL-13-producing nuocytes (type 2 innate lymphoid cells) and airway contraction. J Allergy Clin Immunol 132: 933–941. [PubMed: 23810766]

KEY POINTS

- In a murine model of lung fibrosis, an ontogeny of inflammatory events was defined
- Mutant *Sftpc*^{I73T} expression caused early lung injury marked by a polycelluar alveolitis
- Depletion of peripheral monocytes was protective from *Sftpc*^{I73T} injury

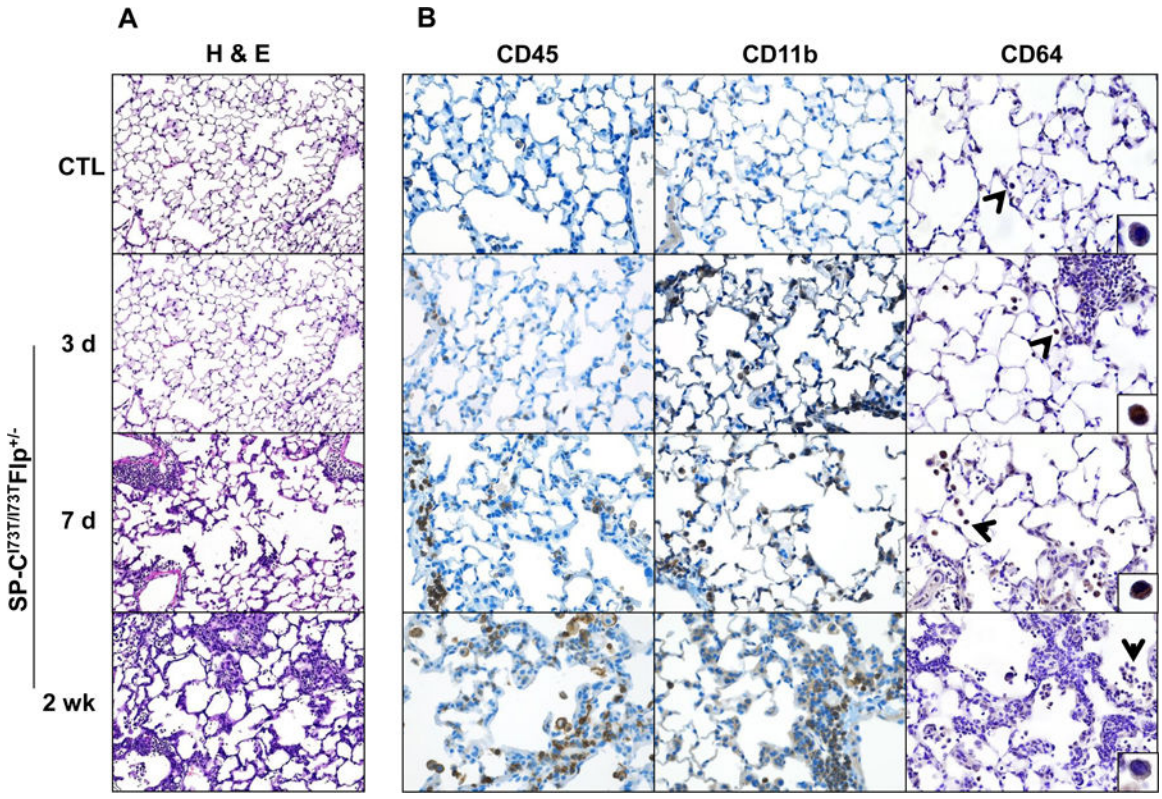

Figure 1. Parenchymal lung injury and alteration in immune cell composition induced by SP-C^{I73T} expression.

(A) High power images of Hematoxylin & Eosin stained sections (100x) of control (tamoxifen treated SP-C$^{WT/WT}$Flp$^{+/+}$ or oil treated SP-C$^{I73T/I73T}$Flp$^{+/-}$ mice) and SP-C$^{I73T/I73T}$Flp$^{+/-}$ mice 3 days, 7 days and 2 weeks following intraperitoneal tamoxifen administration (250 mg/kg). **(B)** Immunohistochemical staining of lungs stained for CD45/ immune cells (left panels), CD11b/migrating cells (center panels) and CD64/mature macrophages (right panels). Magnification: 200x; inset magnification 600x. Images shown are representative of 3–5 animals per group.

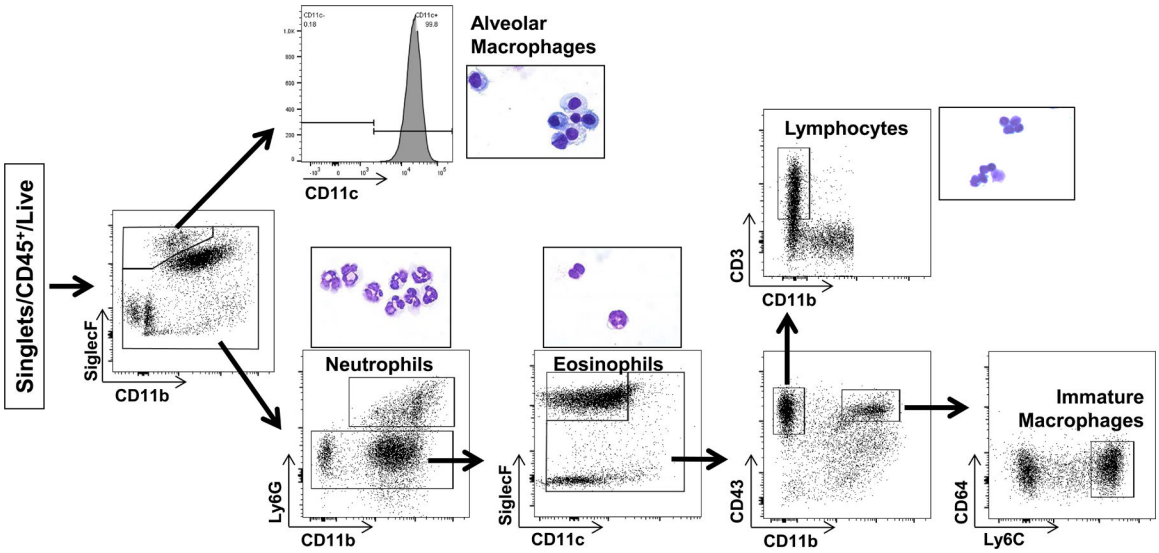

Figure 2. Flow cytometric analysis of CD45^{+} populations in BALF and lung tissue.

Gating strategy used to identify myeloid subsets in control (tamoxifen treated SP-C$^{WT/WT}$Flp$^{+/+}$ or oil treated SP-C$^{I73T/I73T}$Flp$^{+/-}$ mice) and SP-C$^{I73T/I73T}$Flp$^{+/-}$ mice 3 d, 7 d and 2 weeks following intraperitoneal tamoxifen administration (250 mg/kg). BALF and enzymatically digested tissue immune cells were gated on CD45^{+} following exclusion of doublets. Populations were identified based on a modified protocol from Misharin et al., as previously described (9, 20). Alveolar macrophages were gated based SigF^{+}CD11b^{-} expression and confirmed using CD11c, CD64; neutrophils (CD11b^{+}Ly6G^{+}); eosinophils (SigF^{+}CD11b^{+}CD11c^{-}); lymphocytes (CD3^{+}CD11b^{-}); and immature macrophages (CD11b^{+}CD64^{-}Ly6C^{hi}). Insets represent Giemsa stained cytospins of FACS sorted subsets.

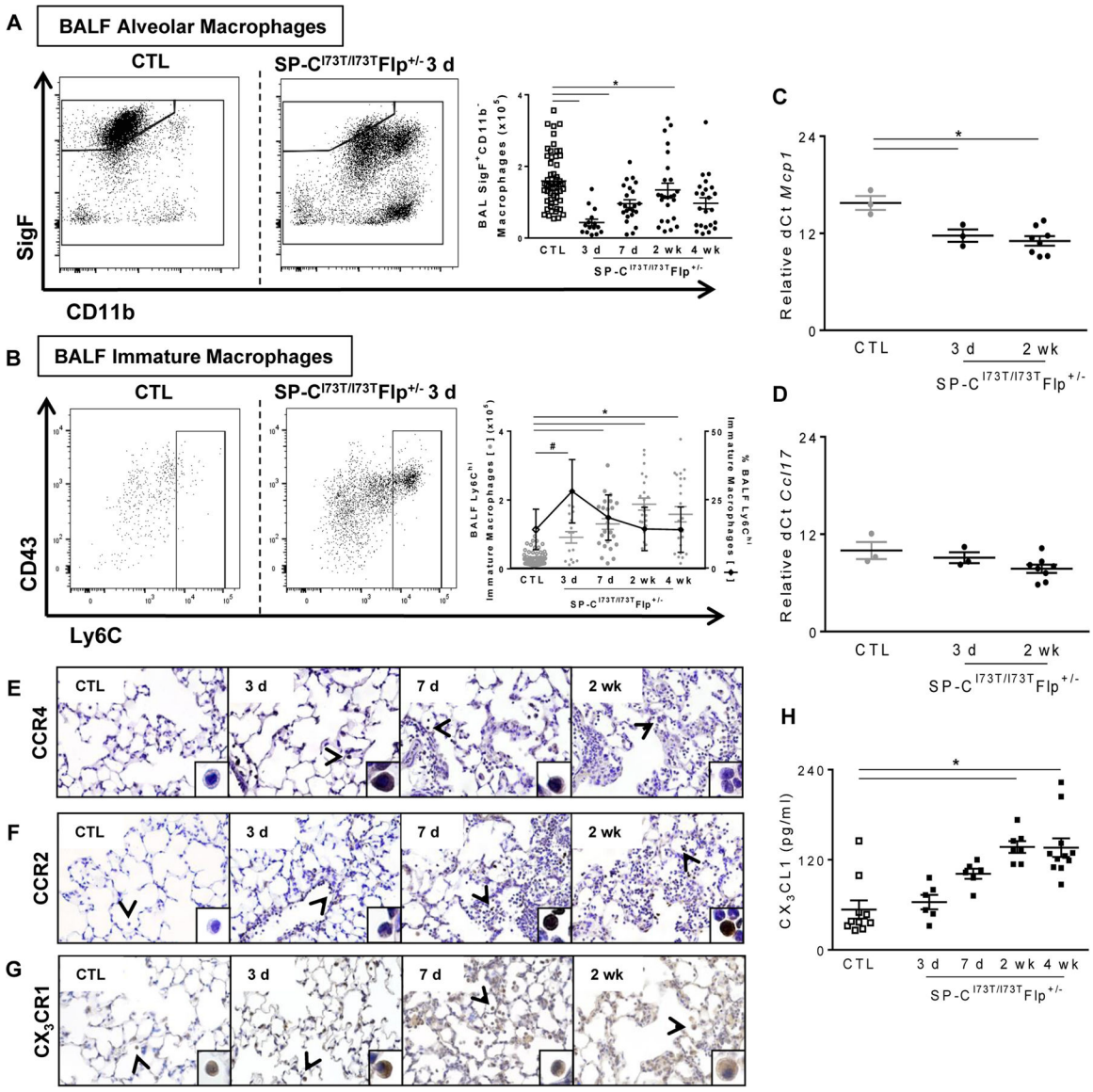

Figure. 3. Characterization of lung macrophage and peripheral monocyte dynamics in SP-C^{I73T} mutant mice.

(A–B) Flow cytometric analysis and quantification of BALF for (**A**) absolute numbers of SigF^{+}CD11c^{+}CD11b^{-} macrophages and (**B**) Ly6C^{+} immature macrophages (absolute numbers left y-axis and relative percentage right y-axis) collected from control (tamoxifen treated SP-C$^{WT/WT}$Flp$^{+/+}$ or oil treated SP-C$^{I73T/I73T}$Flp$^{+/-}$ mice) and SP-C$^{I73T/I73T}$Flp$^{+/-}$ mice 3 d, 7 d, 2 wk and 4 wk following intraperitoneal tamoxifen administration (250 mg/kg). **(C-D)** qPCR analysis of BALF cells collected from control (tamoxifen treated SP-C$^{WT/WT}$Flp$^{+/+}$ or oil treated SP-C$^{I73T/I73T}$Flp$^{+/-}$ mice) and SP-C$^{I73T/I73T}$Flp$^{+/-}$ mice 3 d, and 2 weeks following intraperitoneal tamoxifen administration (250 mg/kg) for markers associated with recruitment of **(C)** monocytes (*Mcp1*) and **(D)** monocyte/macrophages (*Ccl17*). Data are represented as mean ± SEM (N=3–8). * $p < 0.05$ compared to control SP-C$^{WT/WT}$Flp$^{+/+}$ or oil treated SP-C$^{I73T/I73T}$Flp$^{+/-}$ mice SP-C$^{I73T/I73T}$ER$^{-/-}$ by One-Way ANOVA, using Tukey post-hoc test. **(E-G)** Immunohistochemical staining of lungs stained

for **(E)** CCR4, **(F)** CCR2 and **(G)** CX_3CR1 at the indicated time points showing prominent monocyte/macrophage staining (arrowheads). Note peak expression for CCR4 3 d post mutant induction, and time dependent increases in numbers of $CCR2^+$ and CX_3CR1^+ macrophages. Magnification: 200x; inset magnification: 600x. Representative images are shown (N=4). **(H)** CX_3CL1 ELISA of BALF from control (tamoxifen treated SP-$C^{WT/WT}Flp^{+/+}$ or oil treated SP-$C^{I73T/I73T}Flp^{+/-}$ mice) and SP-$C^{I73T/I73T}Flp^{+/-}$ mice 3 d, and 2 weeks following intraperitoneal tamoxifen administration (250 mg/kg). Data are represented as mean ± SEM (N=6–11). Controls were pooled from controls at all 3 time points. *$p < 0.05$ versus control group using 1-way ANOVA followed by Tukey's post hoc test.

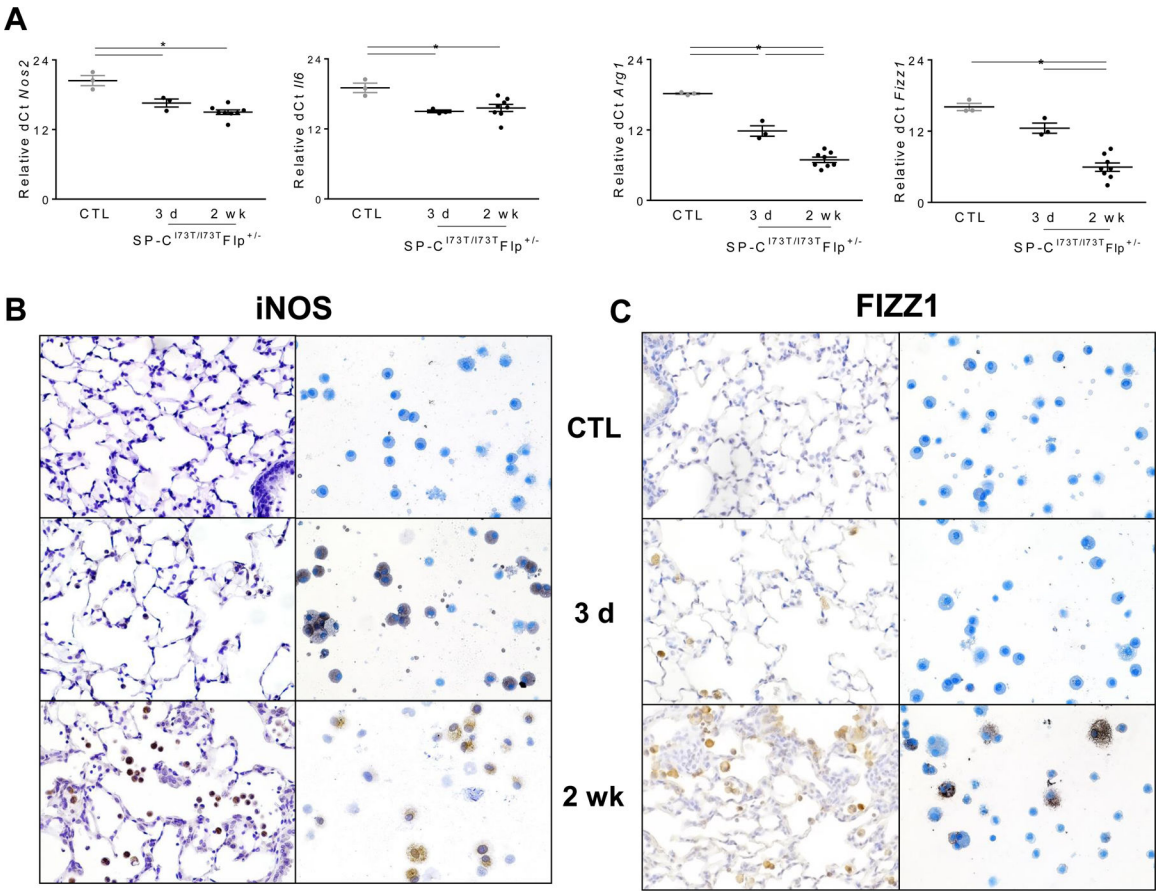

Figure 4. Phenotypic shift of BALF cells following SP-C^{I73T}–induced injury.

(A) qPCR analysis of BALF cells collected from control (tamoxifen treated SP-C$^{WT/WT}$Flp $^{+/+}$ or oil treated SP-C$^{I73T/I73T}$Flp$^{+/-}$ mice) and SP-C$^{I73T/I73T}$Flp$^{+/-}$ mice 3 d, and 2 wk following intraperitoneal tamoxifen administration (250 mg/kg) for markers associated with M1 (*Nos2* and *Il6*) and M2 (*Arg1*, *Fizz1*) activation. Data are represented as dCt relative to 18s and shown as mean ± SEM (N=3–6). *p< 0.05 compared to control SP-C$^{WT/WT}$Flp$^{+/+}$ or oil treated SP-C$^{I73T/I73T}$Flp$^{+/-}$ mice SP-C$^{I73T/I73T}$ER$^{-/-}$ by One-Way ANOVA, followed by Tukey post-hoc test. **(B-C)** Immunohistochemical and cytospin staining of lungs for **(B)** iNOS and **(C)** FIZZ-1. Representative images are shown (200x; N=3–5) from control (tamoxifen treated SP-C$^{WT/WT}$Flp$^{+/+}$ or oil treated SP-C$^{I73T/I73T}$Flp$^{+/-}$ mice) and SP-C$^{I73T/I73T}$Flp$^{+/-}$ mice 3 d and 2 wk following intraperitoneal tamoxifen administration (250 mg/kg).

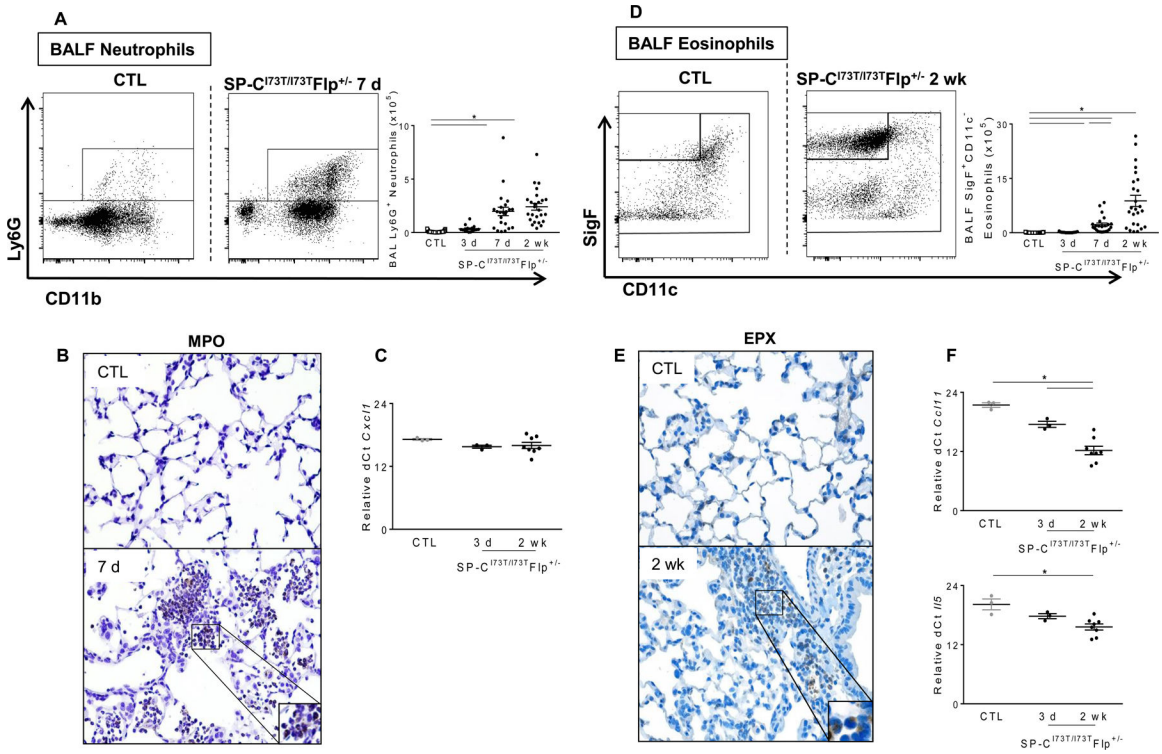

Figure 5. Characterization of BALF neutrophil and eosinophil recruitment in SP-C^{I73T} mutant mice.

Flow cytometric analysis and quantification of BALF **(A)** Ly6G^{+} neutrophil and **(D)** SigF $^{+}$CD11c^{-} eosinophil subsets collected from BALF in control (tamoxifen treated SP-C$^{WT/WT}$Flp$^{+/+}$ or oil treated SP-C$^{I73T/I73T}$Flp$^{+/-}$ mice) and SP-C$^{I73T/I73T}$Flp$^{+/-}$ mice 3 d, 7 d, 2 wk and 4 wk following intraperitoneal tamoxifen administration (250 mg/kg). Absolute quantitation was performed by multiplying the relative abundance of each myeloid subset by the BALF cell counts. Data are represented as mean ± SEM (N=25–51). Immunohistochemical staining of lungs stained for **(B)** myeloperoxidase and **(E)** eosinophil peroxidase (EPX). Magnification: 200x; inset magnification 600x. Representative images are shown (N=3–5). qPCR analysis of BALF cells collected from control (tamoxifen treated SP-C$^{WT/WT}$Flp$^{+/+}$ or oil treated SP-C$^{I73T/I73T}$Flp$^{+/-}$ mice) and SP-C$^{I73T/I73T}$Flp$^{+/-}$ mice 3 d, and 2 weeks following intraperitoneal tamoxifen administration (250 mg/kg) for markers associated with **(C)** neutrophil (*Cxcl1*) and **(F)** eosinophil (*Eotaxin/Ccl11* and *Il5*) recruitment. *p<0.05 compared to control SP-C$^{WT/WT}$Flp$^{+/+}$ or oil treated SP-C$^{I73T/I73T}$Flp $^{+/-}$ mice SP-C$^{I73T/I73T}$Flp$^{-/-}$ by One-Way ANOVA, followed by Tukey post-hoc test.

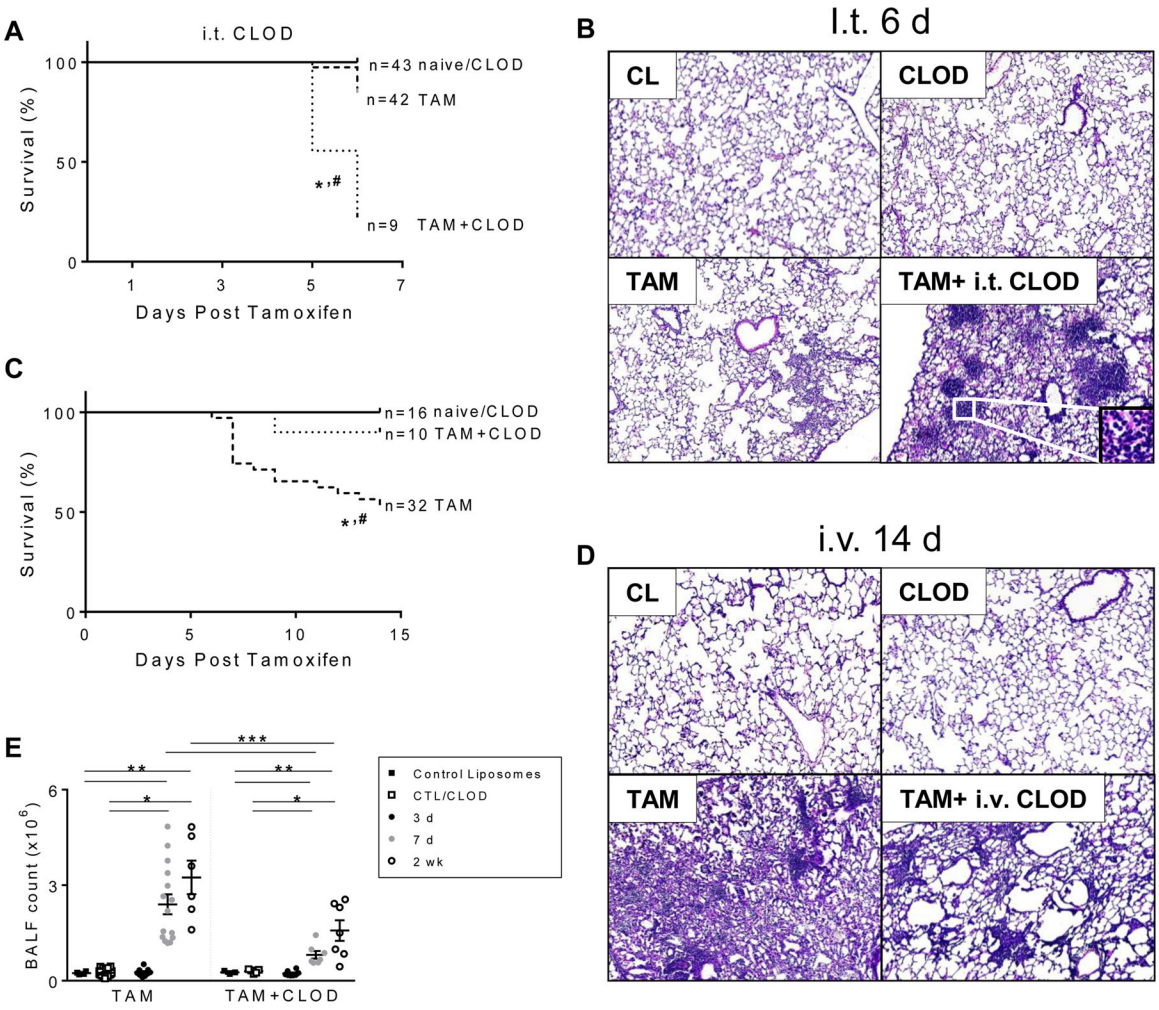

Figure 6. The effect of depletion of alveolar macrophages or peripheral monocytes with clodronate liposomes on lung injury and survival of SP-C^{I73T} mutant mice is dependent upon route of administration.

Kaplan–Meier survival analysis from control (tamoxifen treated SP-C$^{WT/WT}$Flp$^{+/+}$ or oil treated SP-C$^{I73T/I73T}$Flp$^{+/-}$ mice) and tamoxifen induced (250 mg/kg; i.p.) SP-C$^{I73T/I73T}$Flp$^{+/-}$ mice following **(A)** intratracheal (50ul/mouse given 48h prior to induction) or **(C)** intravenous (150 μg/kg given 2 h post induction) clodronate (CLOD) or control (CL) liposome administration (N=3 for control liposome group collected at terminal day; n =10–32 for all other groups). Mean survival using death or body weight < 75% on 2 consecutive days as endpoints is shown. *p<0.05 compared to control mice; #p<0.05 compared to tamoxifen treated mice by Log-Sum (Mantel-Cox) Rank test.

Hematoxylin & Eosin stained sections (40x) from SP-C^{I73T} cohorts treated with i.t. or i.v. clodronate as indicated. **(B)** i.t. CL treated control mice, i.t. CLOD treated control mice or SP-C$^{I73T/I73T}$Flp$^{+/-}$ mice 6 days following TAM induction alone or TAM plus i.t. CLOD as labeled. Representative images are shown (N=1–5). **(D)** i.v. CL treated control mice, CLOD treated control mice or SP-C$^{I73T/I73T}$Flp$^{+/-}$ mice 6 days following TAM induction alone or TAM plus i.v. CLOD. Representative images are shown (N=4–5).

(E) BALF cell counts from SP-C$^{I73T/I73T}$Flp$^{+/-}$ mice (N =10–32) harvested 3 days, 7 days and 2 weeks after tamoxifen ("TAM") induction. A "TAM + CLOD" group was co-treated with intravenous CLOD liposomes (150 μg/kg administered at 2 hours post tamoxifen). Control mice (tamoxifen treated SP-C$^{WT/WT}$Flp$^{+/+}$ or oil treated SP-C$^{I73T/I73T}$Flp$^{+/-}$ mice) received intravenous CLOD or CL liposomes (150 μg/kg administered at 2 hours post tamoxifen or oil injection) as indicated. Data are represented as mean ± SEM (N=3 for each control liposome group harvested at terminal day; N=8–18 for all other groups). *$p<0.05$ compared to control SP-C$^{WT/WT}$Flp$^{+/+}$ or oil treated SP-C$^{I73T/I73T}$Flp$^{+/-}$ mice; **$p<0.05$ compared to tamoxifen treated SP-C$^{I73T/I73T}$Flp$^{+/-}$ mice by One-Way ANOVA, using Tukey post-hoc test.

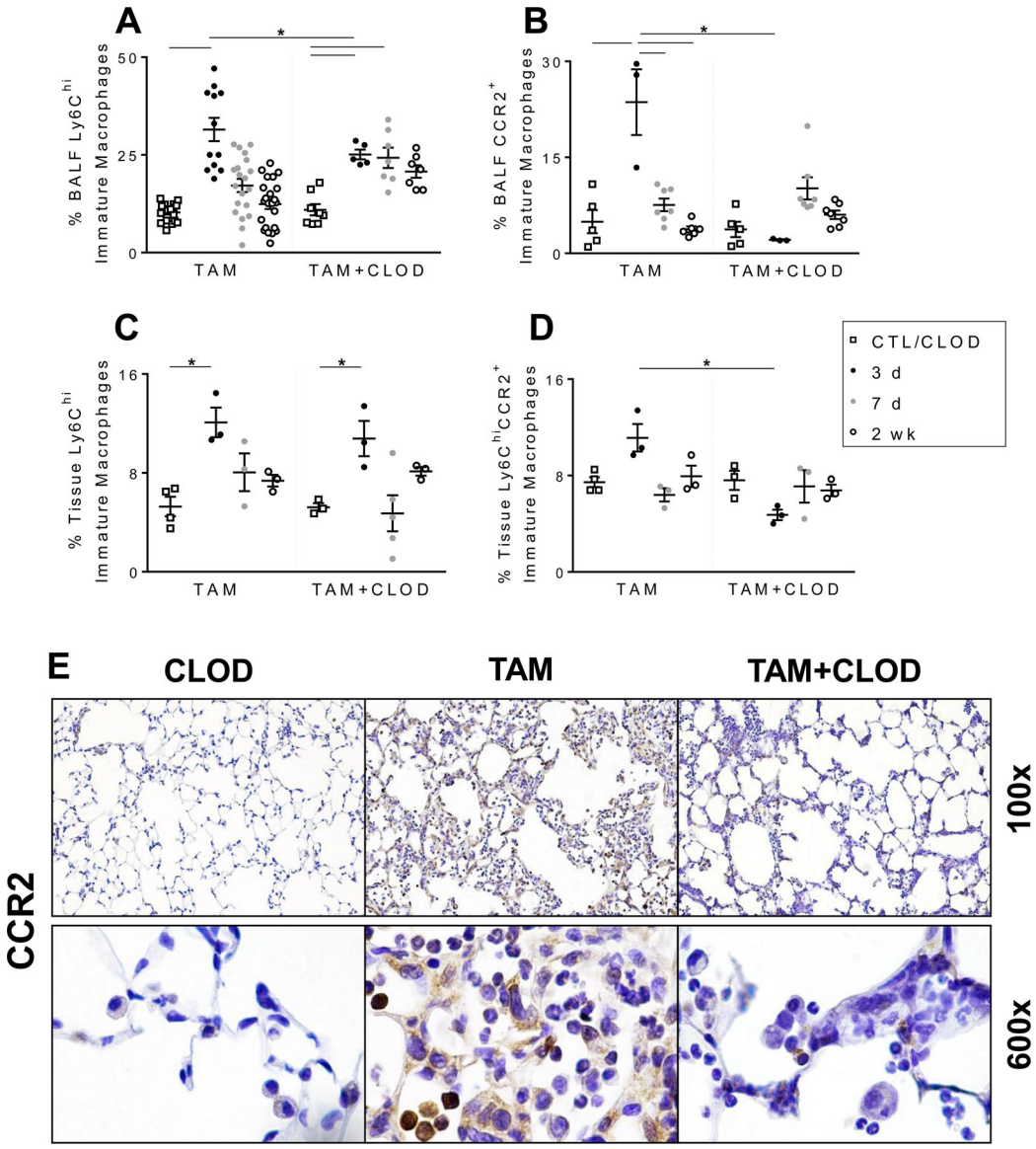

Figure 7. Intravenous monocyte depletion with clodronate liposomes results in altered monocyte/macrophage composition in SP-C^{I73T} mice.

(A; C) Changes in relative percentage Ly6C^{hi} immature macrophages in BALF (**A**) and lung tissue (**C**) from control (tamoxifen treated SP-C$^{WT/WT}$Flp$^{+/+}$ or oil treated SP-C$^{I73T/I73T}$Flp$^{+/-}$ mice) and SP-C$^{I73T/I73T}$Flp$^{+/-}$ mice 3 d, 7 d and 2 weeks following intraperitoneal tamoxifen (250 mg/kg) and intravenous clodronate (150 μg/kg, 2 hours post tamoxifen injection) administration. Data are represented as mean ± SEM (N=5–12).

(B; D) Changes in relative percentage of Ly6C^{hi}CCR2^{+} immature macrophages in BALF (**B**) and tissue (**D**) from control (tamoxifen treated SP-C$^{WT/WT}$Flp$^{+/+}$ or oil treated SP-C$^{I73T/I73T}$Flp$^{+/-}$ mice) and SP-C$^{I73T/I73T}$Flp$^{+/-}$ mice 3 d, 7 d and 2 weeks following intraperitoneal tamoxifen (250 mg/kg) and intravenous clodronate (150 μg/kg, 2 h post tamoxifen injection) administration. Data are represented as mean ± SEM (N=3–8). All analysis was considered significant *p< 0.05 compared to control SP-C$^{WT/WT}$Flp$^{+/+}$ or oil

treated SP-$C^{I73T/I73T}Flp^{+/-}$ mice SP-$C^{I73T/I73T}Flp^{-/-}$ by One-Way ANOVA, using Tukey post-hoc test.

(E) Representative immunohistochemical staining for CCR2 expression of lung sections from SP-C^{I73T} mice (4 lungs/condition) harvested 14 days after tamoxifen induction with ("TAM + CLOD") or without ("TAM") clodronate co-treatment as indicated. "CLOD" represents SP-$C^{WT/WT}Flp^{+/+}$ control mice co-treated with clodronate alone.

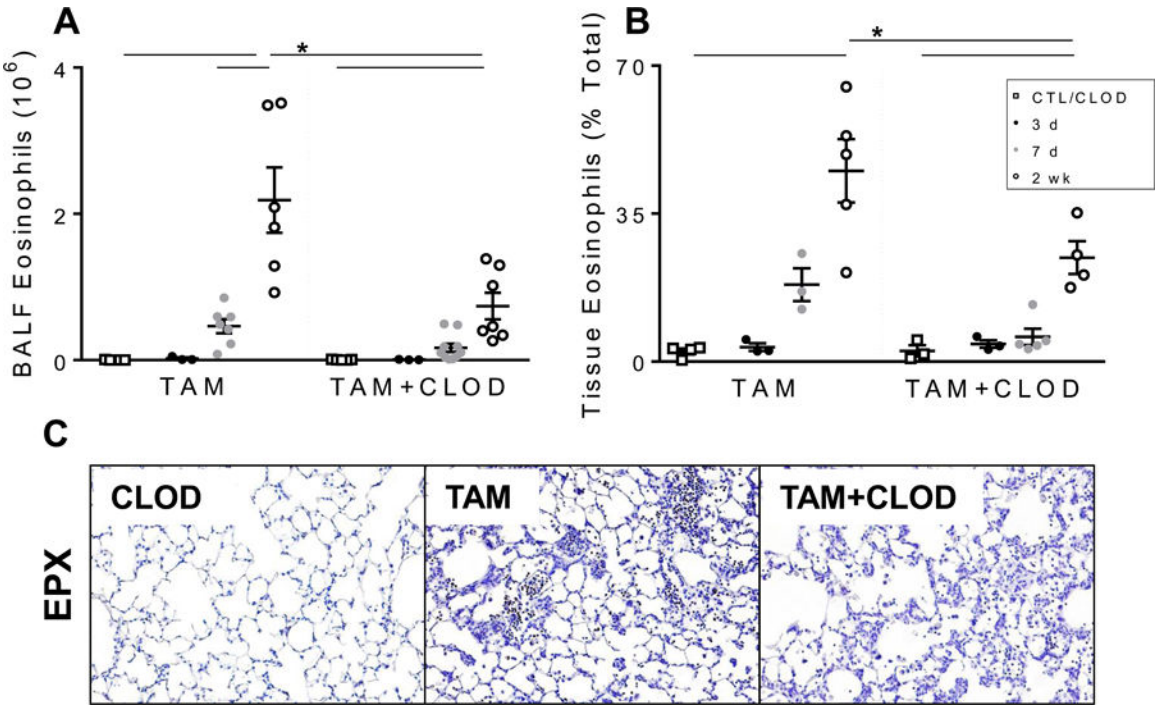

Figure 8. Peripheral monocyte depletion with intravenous clodronate liposomes results in altered eosinophil numbers in SP-C^{I73T} mice.

(A-B) Changes in BAL and tissue SigF^{hi}CD11b^{+}CD11c^{-} eosinophils from control (tamoxifen treated SP-C$^{WT/WT}$Flp$^{+/+}$ or oil treated SP-C$^{I73T/I73T}$Flp$^{+/-}$ mice) and SP-C$^{I73T/I73T}$Flp$^{+/-}$ mice 3 d, 7 d and 2 weeks following intraperitoneal tamoxifen (TAM, 250 mg/kg) and intravenous clodronate (CLOD, 150 μg/kg, 2 h post tamoxifen injection) administration. Data are represented as mean ± SEM (N=3–8). All analysis was considered significant *p< 0.05 compared to control SP-C$^{WT/WT}$Flp$^{+/+}$ or oil treated SP-C$^{I73T/I73T}$Flp$^{+/-}$ mice SP-C$^{I73T/I73T}$ER$^{-/-}$ by One-Way ANOVA, using Tukey post-hoc test. **C)** Immunohistochemical analysis of vehicle and clodronate (150 μg/kg) treated control (tamoxifen treated SP-C$^{WT/WT}$Flp$^{+/+}$ or oil treated SP-C$^{I73T/I73T}$Flp$^{+/-}$ mice) and SP-C$^{I73T/I73T}$Flp$^{+/-}$ mice 2 weeks following intraperitoneal tamoxifen administration (250 mg/kg) lungs stained for eosinophil peroxidase (EPX). Representative 40x images from 3–5 separate animals at each condition are shown.

Table 1.

Tissue inflammation, injury and lung mechanics.

Summary analysis for BALF protein content, BALF cell counts and in vivo pulmonary function testing (inspiratory capacity, static compliance and tissue damping) from control (tamoxifen treated SP-C$^{WT/WT}$Flp$^{+/+}$ or oil treated SP-C$^{I73T/I73T}$Flp$^{+/-}$ mice) and tamoxifen treated (250 mg/kg;i.p.) SP-C$^{I73T/I73T}$Flp$^{+/-}$ mice at 3 d, 7 d and 2 wk. Note that control data represents pooled data from 3 d (N=3), 7 d (N=4), and 2 wk (N=4). Data is represented as mean ± SEM.

Table 1		Protein Content (μg/ml)	Cell Count (10^6)	Inspiratory Capacity (ml)	Static Compliance (ml/cm$_{H2O}$)	Tissue Damping (G, cmH$_2$O/ml)
	CTL (N=11)	438.2 ± 38.3	0.26 ± 0.02	0.74 ± 0.02	0.067 ± 0.002	4.59 ± 0.15
SP-C$^{I73T/I73T}$Flp$^{+/-}$	**3 d (N=8)**	455.9 ± 61.6	0.19 ± 0.03	0.66 ± 0.03	0.057 ± 0.003	5.11 ± 0.28
	7 d (N=7)	2266.6 ± 422.5 *	0.99 ± 0.18 *	0.51 ± 0.05 *	0.040 ± 0.005 *	7.62 ± 0.74 *
	2 wk (N=14)	2245.2 ± 245.0 *	2.66 ± 0.32 *	0.46 ± 0.03 *	0.031 ± 0.004 *	8.84 ± 1.35 *

* $p < 0.05$ compared to control SP-C$^{WT/WT}$Flp$^{+/+}$ or oil treated SP-C$^{I73T/I73T}$Flp$^{+/-}$ mice SP-C$^{I73T/I73T}$ER$^{-/-}$ by ANOVA, using Tukey post-hoc test.